Forward and Reverse Link Constraints in UHF RFID with Passive Tags

Daniel G. Kuester*†[1], David R. Novotny*[2], and Jeffrey R. Guerrieri*[3]
* *National Institute of Standards and Technology*
325 Broadway, Boulder, Colorado 80305, USA
[1] daniel.kuester@nist.gov
[2] david.novotny@nist.gov
[3] jeffrey.guerrieri@nist.gov
† *Electrical, Computer, and Energy Engineering Department*
University of Colorado, Boulder, CO 80309

***Abstract*—This paper examines the relative roles of the forward and reverse links in determining the operational range of passive UHF RFID systems. Simple free space examples in free space show when the forward or reverse link may be the main range constraint in practical systems, depending on reader and tag characteristics. Measurements of transmission and scattering off of a dipole in a real environment demonstrate showed different multipath effects; transmission power fading squared disagreed with backscattered fading in the test environment by up to 8 dB within a measurement range of 2 m.**

I. Introduction

In radio frequency identification (RFID) systems, successful object tracking depends on reliable radio links between readers and tags. A simple strategy to improve link robustness is to increase reader transmit power, but this may waste energy, impose interference on other communication systems, or cause electromagnetic compatibility problems with other electronics [1]. Achieving a balance between these concerns requires an understanding of wireless link behavior in RFID systems.

In most other two-way digital wireless communication systems, signals in each link are transmitted from separate antennas, and propagation losses between them exhibit reciprocity [2]. Forward (reader to tag) links in RFID systems are like this; the reader transmits signals to the tag (although the tags' use of the signal as a power source is relatively novel). In the reverse link, a tag modulates its antenna load impedance to encode information into reflections returned to the reader; this link is physically different, because it is based on scattering and not transmission. The relationship between the scattered signal received at the reader and the transmitted link to the tag is well understood in the free field, but not in practical deployment environments with multipath effects.

Existing literature has examined link performance of this type of system in realistic deployment environments. Forward link propagation models and simulations have been compared with experiment by Mayer *et al* [3], Wang *et al* [4], Jeon [5], Su, *et al* [6], and Jung *et al* [7]. These papers don't, however, address the fundamental relationship between multipath fading in these systems' forward and reverse links. If the fading trends of the two links in the presence of multipath are different, then either one might fade out separately and prevent communication between the reader and tag, which represents a concern for system reliability.

In this paper, we investigate the relationship between the links. As a first approximation, existing free-field models of the forward and reverse links are compared, with some discussion about which is the constraining link in a realistic system. Measurements of transmission and scatter links are presented to compare multipath fading effects in a semi-anechoic chamber and a more reverberant environment. The target "tag" is a Roberts dipole. To measure the reader-to-tag transmission link, a scattering parameter through measurement is taken between it and the "reader" antenna. The tag-to-reader scattered link is simulated by subtracting reflection *S*-parameters of (1) the dipole with a shorted load from (2) the same environment without the dipole; this, like the calibration procedure used in the UHF RFID testing standard ISO 18047-6 [8], includes effects from both structural and antenna mode scattering.

II. Far-field system performance in free space

The symbols used in this paper for far-field system performance is outlined in Table I. In real deployments, these parameters can vary with signal parameters, doppler shift, tag

TABLE I
Link symbols

Modulated, continuous-wave power received at reader	$P_{rx}^{(mod)}$, $P_{rx}^{(cw)}$
Reader transmit power	P_{tx}
Power received at tag	P_{tag}
Reader, tag antenna isotropic gains	G_{rd}, G_{tag}
Wavelength, reader-tag separation	λ, R
Free-field forward, reverse link range	$R_{\rightarrow}, R_{\leftarrow}$
Threshold activation power density of tag	$W_{tag,th}$
Reader receive sensitivity threshold	$P_{rx,th}^{(mod)}$
Reader, tag impedance mismatch power losses	e_{rd}, e_{tag}
Polarization mismatch power loss	e_{pol}

damage or deterioration, and tag antenna detuning. Some of these are addressed in other papers (e.g., [9]).

A. The forward link

A simple reader-to-tag transmission model is the far-field Friis transmission equation [2]

$$P_{tag} = P_{tx} G_{tag} G_{rd} e_{tag} e_{rd} e_{pol} \left(\frac{\lambda}{4\pi R} \right)^2, \tag{1}$$

where each variable except R depends on frequency. P_{tag}, e_{pol}, G_{tag}, and G_{rd} also vary with the antennas' relative orientation.

Power received by the tag must exceed a threshold $P_{tag,th}$ to turn on, corresponding to an incident power density of $W_{tag,th} = P_{tag,th}/(\lambda^2 G_{tag} e_{tag})$ [2]. An equivalent "tag sensitivity" that is often used in industry [9] is $\lambda^2 W_{tag,th}$. This threshold in terms of (1) is

$$P_{tx} G_{rd} e_{rd} e_{pol} \left(\frac{\lambda}{4\pi R} \right)^2 \geq \lambda^2 W_{tag,th}. \tag{2}$$

Because power delivered in this model decreases monotonically, a maximum forward link range $R_{\rightarrow}$ is

$$R_{\rightarrow} = \left(\frac{P_{tx}}{\lambda^2 W_{tag,th}} G_{rd} e_{rd} e_{pol} \right)^{1/2} \frac{\lambda}{4\pi}. \tag{3}$$

B. The reverse link

The scattered continuous-wave power $P_{rx}^{(cw)}$ received at the reader from an object with a radar cross-section σ can be estimated in the far field with the monostatic radar equation [2]:

$$P_{rx}^{(cw)} = P_{tx} (G_{rd} e_{rd} e_{pol})^2 \frac{\lambda^2}{(4\pi)^3 R^4} \sigma. \tag{4}$$

If the target is a tag modulating its antenna load impedance between two states creating a modulated "delta" or "differential" radar cross-section $\Delta\sigma$, then a corresponding modulated power received at the reader $P_{rx}^{(mod)}$ is

$$P_{rx}^{(mod)} = P_{tx} (G_{rd} e_{rd} e_{pol})^2 \frac{\lambda^2}{(4\pi)^3 R^4} \Delta\sigma. \tag{5}$$

A convenient and equivalent expression for link calculations uses a "tag scattering loss" defined as $\chi = 4\pi\Delta\sigma/\lambda^2$ so that

$$P_{rx}^{(mod)} = P_{tx} (G_{rd} e_{rd} e_{pol})^2 \left(\frac{\lambda}{4\pi R} \right)^4 \chi. \tag{6}$$

Both $\Delta\sigma$ and χ depend not only on relative polarization, tag orientation, and frequency like $W_{tag,th}$, but also power incident on the tag [10].

If the reader's receive sensitivity is $P_{rd,th}^{(mod)}$, then the reverse link must satisfy

$$P_{tx} (G_{rd} e_{tx} e_{pol})^2 \left(\frac{\lambda}{4\pi R} \right)^4 \chi \geq P_{rx,th}^{(mod)} \tag{7}$$

for a successful link. The maximum reverse-link range $R_{\leftarrow}$ is therefore

$$R_{\leftarrow} = \left[\frac{P_{tx} \chi}{P_{rx,th}^{(mod)}} \right]^{1/4} (G_{rd} e_{rd} e_{pol})^{1/2} \frac{\lambda}{4\pi} \tag{8}$$

in free space.

C. System performance

As a case study, recent tags' $W_{tag,th}$ and χ measured by Nikitin and Rao [9] are shown in Fig. 1. Free-field read

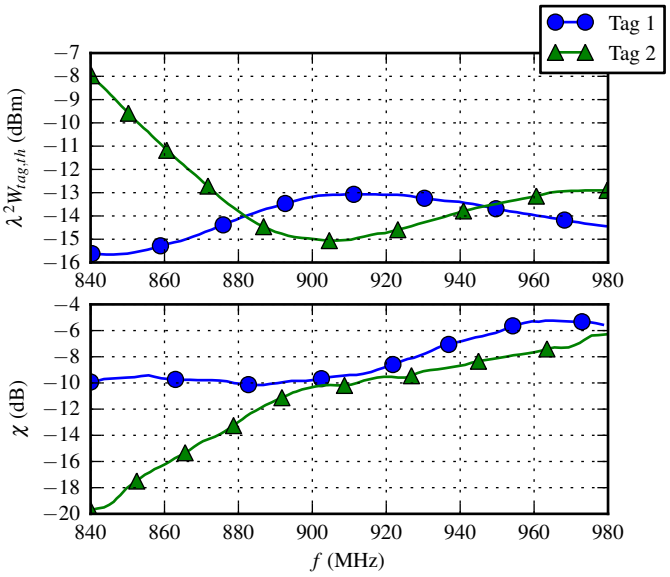

Fig. 1. Nikitin and Rao's characterization [9] of the sensitivity $\lambda^2 W_{tag,th}$ and backscattering factor χ of two commercially available tags. The tags were oriented broadside toward the reader antenna, and interrogated with the "case A" signal parameters.

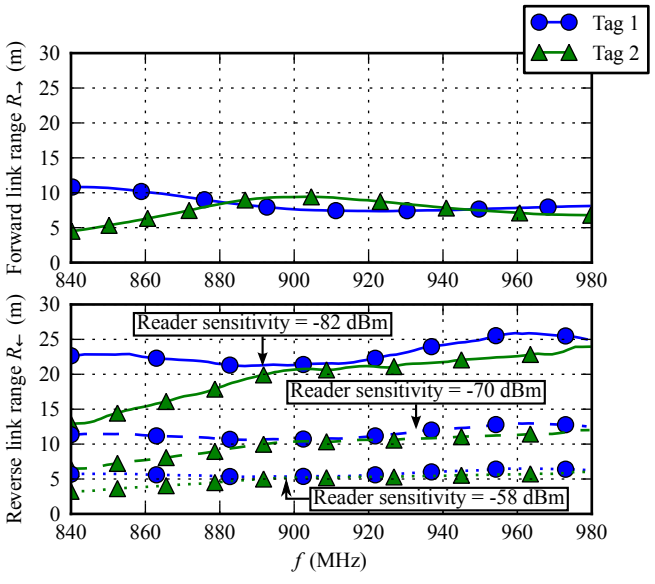

Fig. 2. System range estimates of the tags in Fig. 1 positioned the far field and free space. The estimates use (3) and (8), with $P_{tx} = 28$ dBm, matched impedances and polarizations, and $G_{rd} = 8$ dBi. The reverse link is shown with some example reader sensitivities $P_{rd,th}^{(mod)}$.

range estimates from (3) and (8) with a reader radiating $P_{tx} = 28$ dBm are shown in Fig. 2.

The assumption (as in [3]-[7]) that the overall system read range is limited by $R_{\rightarrow}$ can be checked by comparing it against $R_{\leftarrow}$. A figure of merit can be defined as the ratio of (3) and (8):

$$\frac{R_{\rightarrow}}{R_{\leftarrow}} = \left[\frac{P_{tx} P_{rd,th}^{(mod)}}{\chi (\lambda^2 W_{tag,th})^2} \right]^{1/4}, \tag{9}$$

which is less than one if the forward link is the main constraint. Interestingly, this quantity is independent of antenna properties for monostatic systems.

Values of $R_{\rightarrow}/R_{\leftarrow}$ from Fig. 2 at 915 MHz are shown in Table II. Note that the forward link is only the constraining link in this free-field model if the reader's receive sensitivity is better than -66 dBm.

If tag sensitivities continue to improve, then (9) shows that the reverse link will become a more important constraint. Even if tag advances improve χ at about the same short term rate, the $(\lambda^2 W_{tag,th})^2$ term will still fall faster, and the reverse link will still continue to become more important.

III. Link Performance with Multipath

This section presents measured UHF scattering and transmission behavior in both a semi-anechoic environment and a more reverberant indoor storage environment to investigate multipath fading performance.

A. Measurement technique

To mitigate measurement complexity associated with RFID protocol signaling, measurements were performed on a network analyzer with continuous wave signals. These signals were assumed to be similar enough to the narrowband signaling in UHF RFID systems to exhibit the same propagation behavior. Two commercially available 902-928 MHz 8 dBi RFID reader antennas were chosen: one was linear polarized (LP), and the other circular polarized (CP). A Roberts dipole [11] tuned to 915MHz was chosen as the "tag" target to resemble dipole-based designs used in common tags. The reflection coefficients of the antennas are shown in Fig. 3.

Measurements were performed in each configuration shown in Fig. 4. First, a transmission measurement is performed to imitate a passive RFID forward link, with S-parameters calibrated as shown in Fig. 4a; the recorded value is $|S_{21}|^2 = P_{tag}/P_{tx}$ (the value modeled in (1) for the free-field case). Figure 4b shows the procedure used to measure the difference detected between tag backscattering states in a reverse link. This is the same approach used for the cross-section measurement calibration outlined in ISO/IEC 18047-6, with the $\lambda/2$ Roberts dipole shorted (and leaving its feed cable with a matched termination) instead of a $\lambda/2$ rod. The reflection coefficient at one of the "reader" patch antennas is measured in each of the two states of the "tag" simulated in Fig. 4b: the test environment (1) with, then (2) without the shorted dipole and matched feed. The magnitude of the difference between the two values is reported, so that $|\Delta S_{11}|^2 = P_{rx}^{(mod)}/P_{tx}$. The noise floor of $|\Delta S_{11}|$ was better than -75 dB across 700-1100 MHz.

For each set of transmission and scattering measurements, both the patch and dipole antennas were aligned to boreside orientation with a laser square, and co-polarized with a level.

TABLE II
Free-field relative link range figures of merit $R_{\rightarrow}/R_{\leftarrow}$ near 915 MHz for example reader sensitivities, taken from Fig. 2.

$P_{rd,th}^{(mod)}$	$R_{\rightarrow}/R_{\leftarrow}$	Weakest link
-58 dBm	1.6	Reverse
-70 dBm	0.8	Forward
-82 dBm	0.4	Forward

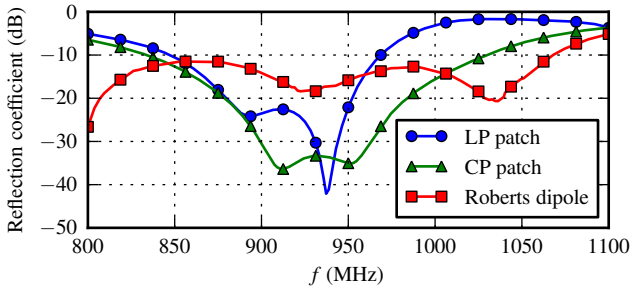

Fig. 3. Reflection coefficients of the three antennas under test. The two patches are commercially available RFID reader patch antennas. The dipole was selected to imitate common tag antennas.

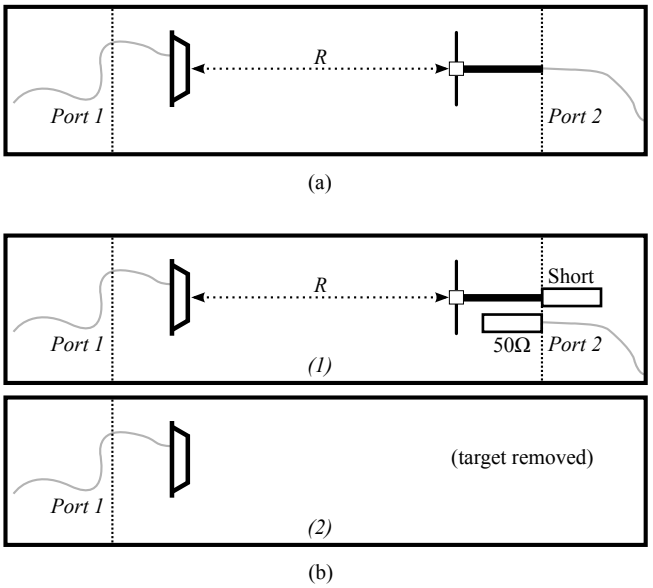

Fig. 4. Measurement setup. In the forward link configuration (a), a full two-port measurement was performed with the network analyzer, calibrated to the S-parameter reference planes shown; measurements of $|S_{21}|^2$ are taken to describe link losses. In the reverse link measurement (b), measurements of the 1-port reflection coefficients are taken with (1) the shorted dipole target (with the feed line from (a) shorted) and (2) the same environment without a target; the magnitude of the difference $|\Delta S_{11}|$ is recorded. This resembles calibration measurements described in ISO/IEC 18047-6 [8].

This procedure was repeated in each environment and for each reader antenna. The range R between the two antennas, shown dotted in Fig. 4, was measured by laser range finder in each experiment.

The dominant contributors to random uncertainty in this measurement are alignment errors and range measurement error, and instrument noise for the reflection measurements. These will be estimated later by repeatability tests. These will be assumed larger than any systematic uncertainties such as effects of reflections in the semi-anechoic chamber or near-field effects at closer ranges.

Measurements were made in the semi-anechoic environment shown in Fig. 5, and in the storage room pictured in Fig. 6 as an example of a reverberant environment.

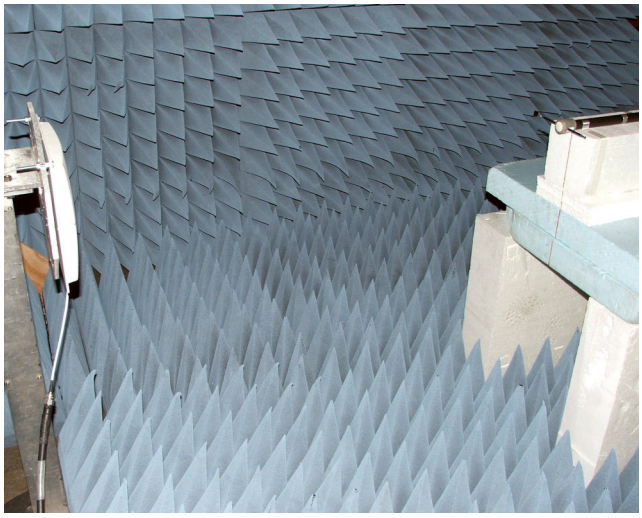

Fig. 5. The measurement setup in the semi-anechoic chamber. The LP reader antenna is shown attached to the mounting structure on the left, and the target dipole is on the right.

Fig. 6. The measurement setup in the reverberant storage environment under test. This room's ceiling, walls, and floor are constructed of steel-reinforced concrete. There is a large window facing outdoors above the frame, a large workbench and wall to the rear, and well-organized shelving containing test equipment on the right and left.

B. Measurement results

Measurements of scattering and throughput in the semi-anechoic chamber $|\Delta S_{11}^{(an)}|$ and $|S_{21}^{(an)}|$ are plotted against range R in Fig. 7 at either end of the 902-928 MHz band. Regressions to $1/R^2$ and $1/R^4$ accounting for apparent phase centers are

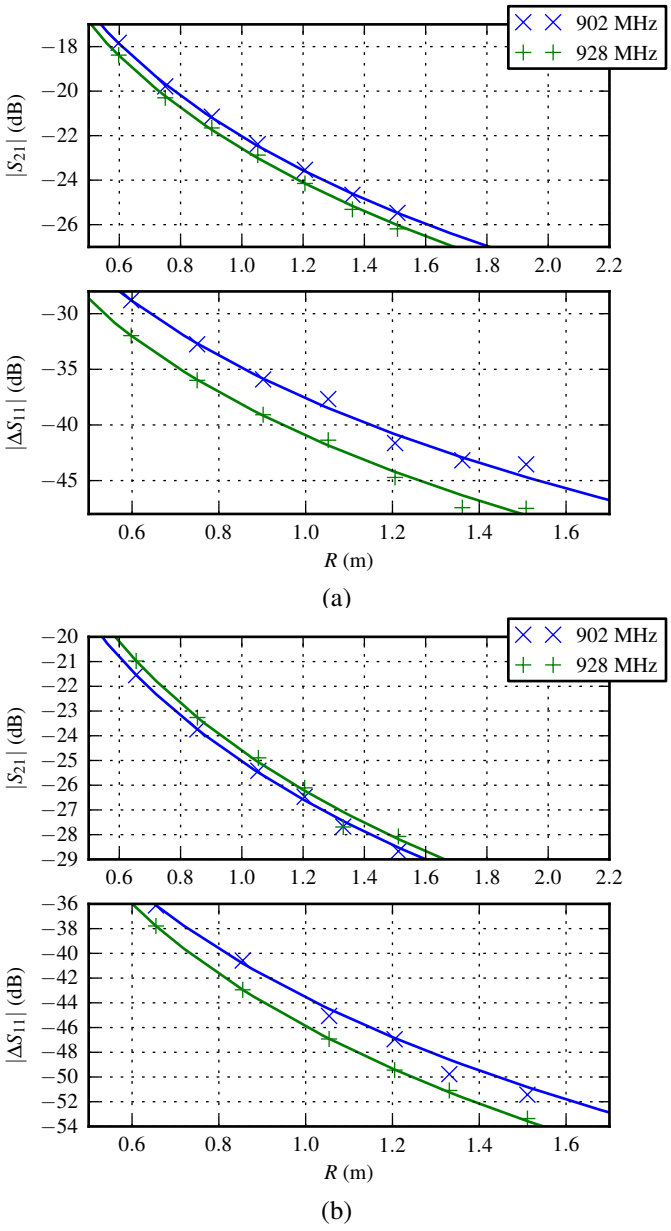

Fig. 7. Throughput and scattering measurements against range with (a) the 8 dBi LP patch and (b) the 8 dBi CP patch antennas. The curves are fitted to R dependences as appropriate in (2) and (6), and to apparent phase centers. Regression information across 895-935 MHz are in Table III.

TABLE III
Regression information from Fig. 7 within 895-935MHz

	$\lvert S_{21}\rvert$		$\lvert\Delta S_{11}\rvert$		*Apparent phase*
	Std. Dev.	*Worst*	*Std. Dev.*	*Worst*	*center offset*
CP patch	0.05 dB	0.24 dB	0.22 dB	1.1 dB	0.008 - 0.049 m
LP patch	0.07 dB	0.23 dB	0.45 dB	1.5 dB	0.042 - 0.059 m

shown to validate the anechoic performance of the chamber; some information about the regression fit quality and apparent phase centers are shown in Table III.

To make the multipath effects clear, results from the storage room environment are normalized to semi-anechoic chamber data in Fig. 8 by means of equations 10 and 11:

$$F_{\rightarrow} = \frac{|S_{21}|^2}{|S_{21}^{(an)}|^2} \tag{10}$$

for the forward link, and

$$F_{\leftarrow} = \frac{|\Delta S_{11}|^2}{|\Delta S_{11}^{(an)}|^2} \tag{11}$$

in the reverse link. $|S_{21}|^2$ and $|\Delta S_{11}|^2$ are measured in the fading test environment (the storage room) the same way as for the semi-anechoic cases.

Figure 8 shows $F_{\rightarrow}$ and $F_{\leftarrow}$ at various distances between the reader antennas and the dipole target in the storage environment shown in Fig. 6. Corresponding uncertainty estimates are shown in Table IV. As R increases, multipath effects tend to become more significant in both links.

Notably, the $F_{\rightarrow}$ and $F_{\leftarrow}$ curves show similar contours, but simply squaring the one-way fading ($F_{\rightarrow}^2$) does not match the reverse link fading $F_{\leftarrow}$. Across all measurements within 895-935 MHz, that discrepancy $F_{\rightarrow}^2/F_{\leftarrow}$ (plotted in Fig. 9) ranged from -6 to +8 dB, which is beyond the 1.3 dB uncertainty estimate.

IV. Conclusion

Measurements presented in this paper have demonstrated the unclear relationship between forward and reverse link multipath fading. Even within a relatively close 2 m reader to tag range, the forward link transmission fading taken twice differed from the scattered fading by up to 8 dB.

There is a key difference between the scattering measurements reported here (as in the calibration against the rod $\lambda/2$ modelled as a in ISO 18047-6) and realistic tags: the latter modulates the antenna load between two states, rather than removing the physical antenna structure entirely. This affects the results presented here, where scattering components from the antenna structure that did not interact with the load ("structural mode" scatter) are detected as well. Future work will examine purely load modulated scattering.

Previous work has discussed the possibility of reducing RFID readers' radiated emissions mitigate interference risks [1]. Fortunately, RFID deployment designers with both interference and link reliability concerns have a variety of options to help achieve both: there is literature about frequency [12], antenna polarization [13] [14], and spatial [15] diversity schemes. In the reverse link, these techniques may help too, and overspecifying reader receive sensitivity may help mitigate fading concerns. Still, system users and installers may choose to set reader power output to the maximum legal levels hoping to improving system reliability, so more work is needed to find a balance between interference potential and link reliability interests.

TABLE IV
Combined uncertainty estimates of random alignment errors and noise at 915 MHz with coverage factor 2.

Measurement	Uncertainty estimate
$\lvert S_{21}\rvert^2$	0.2 dB (at worst case, $R = 0.6$ m)
$\lvert \Delta S_{11}\rvert^2$	0.9 dB (at worst case, $R = 2$ m)
$F_{\rightarrow}$	0.3 dB
$F_{\leftarrow}$	1.2 dB
$F_{\rightarrow}^2/F_{\leftarrow}$	1.3 dB

V. Acknowledgements

The author thanks Pavel Nikitin for granting use of his data, and Randal Direen for his help in constructing the anechoic range.

The Department of Homeland Security Science and Technology Directorate has, in part, sponsored the production of this material with NIST.

References

[1] D.R. Novotny, J.R. Guerrieri, D.G. Kuester, "Potential interference issues between FCC part 15 compliant UHF ISM emitters and equipment passing standard immunity testing requirements," *Proc. 2009 Symp. on Electromagnetic Compatibility*, pp.161-165, 17-21 Aug. 2009.

[2] C.A. Balanis, *Antenna Theory: Analysis and design, 3rd ed*. Hoboken, NJ: Wiley & Sons, 2005, pp. 94-99.

[3] L.W. Mayer, M. Wulich, S. Caban, "Measurements and channel modeling for short range indoor UHF applications," *Proc. 2006 European Conf. on Antennas and Propagation*, pp.1-5, 6-10 Nov. 2006.

[4] H.G. Wang , C.X. Pei, C.H. Zhu, "A link analysis for passive UHF RFID system in LOS indoor environment," *Proc. 4th Intl. Conf. on Wireless Communications, Networking and Mobile Computing (WiCOM)*, pp. 1-7, 2008.

[5] K.Y. Jeon, S.H. Cho, "Performance of RFID EPC C1 Gen2 Anti-collision in multipath Fading Environments," *Proc. 2nd Intl. Conf. on Communication Theory, Reliability, and Quality of Service*, pp. 20-25, Jul. 2009.

[6] W. Su, K.M. Beilke, T.T. Ha, "A reliability study of RFID technology in a fading channel," *Proc. Asilomar Conf. on Signals, Systems, and Computers*, pp. 2124-2127, 4-7 Nov. 2007.

[7] J.-W. Jung, J-H. Hwang, Y.-J. Moon, H.-K. Kwak, H.-H. Roh, J.-S. Park, M.-S. Kang, "Multipath fading measurement on the circularly propagated UHF RFID reader antennas in a practical area", *Proc. Asia-Pacific Symposium on Electromagnetic Compatibility*, pp. 315-318, 19-23 May 2008.

[8] *Radio frequency identification device conformance test methods — Test methods for air interface communications at 860 MHz to 960 MHz*, ISO/IEC standard 18047-6, 2006.

[9] P.V. Nikitin and K.V.S. Rao, "Effect of gen2 protocol parameters on RFID tag performance," *Proc. 2009 Intl. Conf. on RFID*, pp.117-122, 28-29 Apr. 2009.

[10] S. Skali, C. Chantepy, S. Tedjini, "on the measurement of the delta radar cross section (ΔRCS) for UHF tags," *Proc. 2009 Intl. Conf. on RFID*, pp.346-351, 28-29 Apr. 2009.

[11] D. Morgan, *A handbook for EMC testing and measurement*. Institution Of Engineering And Technology, 1994, pp. 92-93.

[12] H.-C. Liu, Y.-T. Chen, W.-S. Tzeng, "A multi-carrier UHF passive RFID system," *Proc. Intl. Symp. on Applications and the Internet Workshops*, pp. 21-24, Jan. 2007.

[13] J.D. Griffin, G.D. Durgin, "Reduced fading for RFID tags with multiple antennas," *Proc. 2007 IEEE Antennas and Propagation Society International Symposium*, pp.1201-1204, 9-15 Jun. 2007.

[14] G.D. Durgin, A. Rohatgi, "Multi-antenna RF tag measurement system using back-scattered spread spectrum," *Proc. 2008 IEEE Intl. Conf. on RFID*, pp. 1-8, 16-17 Apr. 2008.

[15] W. He, Y. Huang, Z. Wang, Y. Zhao, "A circular polarization MIMO antenna system applied for RFID management," *Proc. 2008 Int. Symp. on Antennas, Propagation, and EM Theory*, pp. 225-228, 2-5 Nov. 2008.

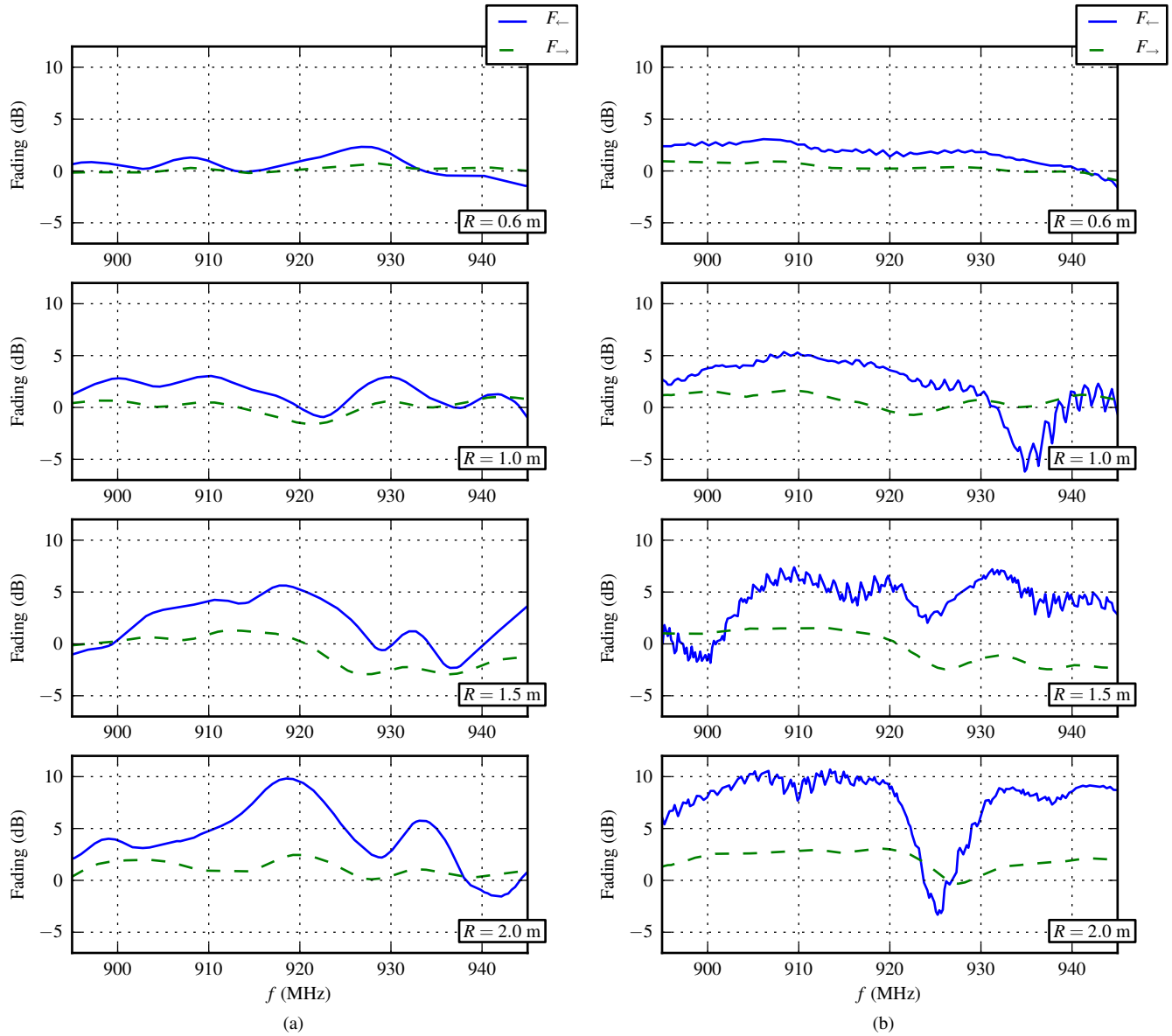

Fig. 8. Multipath fading with the (a) LP and (b) CP patch antennas. The curves show measurements from the reverberant environment (shown in Fig. 6) normalized to the regressions in Fig. 7. Peaks and nulls tend deeper as the separation R between the reader antenna and the target increases.

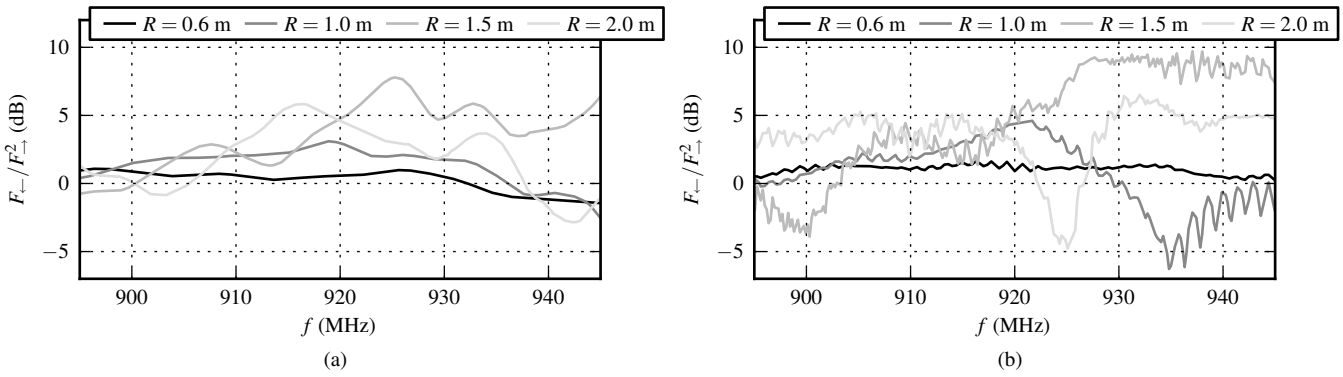

Fig. 9. The discrepancy $F_{\leftarrow}/F_{\rightarrow}^2$ between forward and reverse link fading from measurements taken with the (a) LP and (b) CP patch antennas, computed with the data in Fig. 8. The random uncertainty (from Table IV) in these reported values is estimated to be 1.3dB.